IL NUOVO CIMENTO **47 C** (2024) 11
DOI 10.1393/ncc/i2024-24011-6

COLLOQUIA: La Thuile 2023

Evidence of the off-shell Higgs and Higgs decay width constraints at ATLAS

YINGJIE WEI on behalf of the ATLAS COLLABORATION

University of Oxford - Oxford, UK

received 10 October 2023

Summary. — This paper reports a search for off-shell Higgs boson production and the measurement of the Higgs decay width using the full Run-2 pp collision dataset, corresponding to an integrated luminosity of 139 fb^{-1}, collected by the ATLAS detector at the Large Hadron Collider. In this analysis, the Higgs boson production modes include gluon-gluon fusion, vector-boson fusion, and VH, while the Higgs boson decay channels $ZZ \to 4\ell$ and $ZZ \to 2\ell 2\nu$ ($\ell = e$ or μ) are considered. The background-only hypothesis is rejected at the confidence level of 3.3 σ (2.2 σ) for the observed (expected) result, providing evidence of the off-shell Higgs boson. The combination of the off-shell and on-shell Higgs boson measurements can constrain the Higgs decay width to be $4.5^{+3.3}_{-2.5}$ MeV, with an upper limit of 10.5 MeV at the 95% confidence level.

1. – Introduction

The Higgs boson discovery, reported by ATLAS and CMS [1, 2] at the LHC in 2012, was a milestone in particle physics. Since then, great efforts have been made to measure its properties and couplings to elementary particles [3, 4], as well as BSM searches. A key parameter predicted by the SM is the Higgs boson width (Γ_H). Its expected value (Γ_H^{SM}) is only 4.1 MeV [5], which is three orders of magnitude smaller than the resolution of the ATLAS detector (a few GeV). To address this challenge, an indirect method [6] has been developed to constrain the Higgs width, relying on both on- and off-shell Higgs production.

The on-shell Higgs cross-section is inversely proportional to its width (as seen in $gg \to H \to ZZ$):

$$\sigma^{\text{on-shell}}_{gg\to H\to ZZ} \propto \frac{g^2_{ggH} g^2_{HZZ}}{m_H \Gamma_H}, \tag{1}$$

while the off-shell Higgs production is independent of the Higgs width:

$$\sigma^{\text{off-shell}}_{gg\to H\to ZZ} \propto \frac{g^2_{ggH} g^2_{HZZ}}{m^2_{ZZ}}. \tag{2}$$

Here, g_{ggH} and g_{HZZ} are the Higgs-gluon and Higgs-Z boson couplings, respectively. If these couplings are assumed to be equal between on- and off-shell regions, Γ_H can be measured from the cross-section ratio.

The on-shell Higgs measurement has been conducted [7]. This paper concentrates on the off-shell Higgs production, which contributes $\mathcal{O}(15\%)$ of the total Higgs cross-section, enhanced by two resonances around twice the masses of the Z boson ($2m_Z$) and the top quark ($2m_t$) from the gluon-gluon fusion (ggF) mode. Additionally, this analysis accounts for vector-boson fusion (VBF) and VH production, collectively referred to as EW production, which plays a crucial role, particularly in higher energy regions. The continuum ZZ events from $q\bar{q}$ are the primary background.

This paper reports a search for off-shell Higgs production using the full Run-2 dataset at a centre-of-mass energy of 13 TeV, collected by the ATLAS at the LHC. The final states of Higgs decay to two Z bosons considered in this analysis include 4ℓ and $2\ell 2\nu$.

2. – Analysis

2˙1. *$ZZ \to 4\ell$ Analysis.* – To enhance sensitivity in both ggF and EW production modes, three signal regions (SRs) are defined. SRs include events with $m_{4\ell} > 220$ GeV, while events with $180 < m_{4\ell} < 220$ GeV are considered in control regions (CRs) which have low signal-to-background ratios. The three SRs are categorized primarily based on jet multiplicity. The EW SR contains events with two or more jets and well-separated first two leading jets ($|\eta_{jj}| > 4$). Events with one forward region jet ($|\eta_j| > 2.2$) belong to the mixed SR. Other events are included in the ggF SR.

The primary background in $ZZ \to 4\ell$ is $q\bar{q} \to ZZ$ events. Their normalization is estimated using data in three CRs defined with different jet multiplicities: zero, one, or ≥ 2 jets, for better emulation of SR characteristics. Other backgrounds, such as $gg \to ZZ$, EW $q\bar{q} \to ZZ$, and small backgrounds from tri-boson, $t\bar{t}Z$ are evaluated using simulation.

In the SRs, a multi-class neural network is employed to include information missing in the matrix-element method. The input variables include matrix elements, kinematic information of each lepton and the entire 4ℓ system, and jet information. Two independent neural networks, trained using Keras with TensorFlow as the backend, are constructed to constrain ggF and VBF processes separately. Each neural network distinguishes three classes: non-interfering (NI) background ($q\bar{q} \to ZZ$), the interfering background (B) ($gg \to ZZ$ for the ggF neural network and $q\bar{q} \to ZZ + 2j$ for the VBF neural network) and the Higgs signal (S) (ggF signal for the ggF neural network and $q\bar{q} \to H^* \to ZZ + 2j$ for the VBF neural network).

The final discriminant observable is constructed using the trained scores in each class (P_{S}, P_{I}, and P_{NI}) as follows:

$$\mathcal{O}_{\text{NN}} = \log_{10}\left(\frac{P_{\text{S}}}{P_{\text{I}} + P_{\text{NI}}}\right) \tag{3}$$

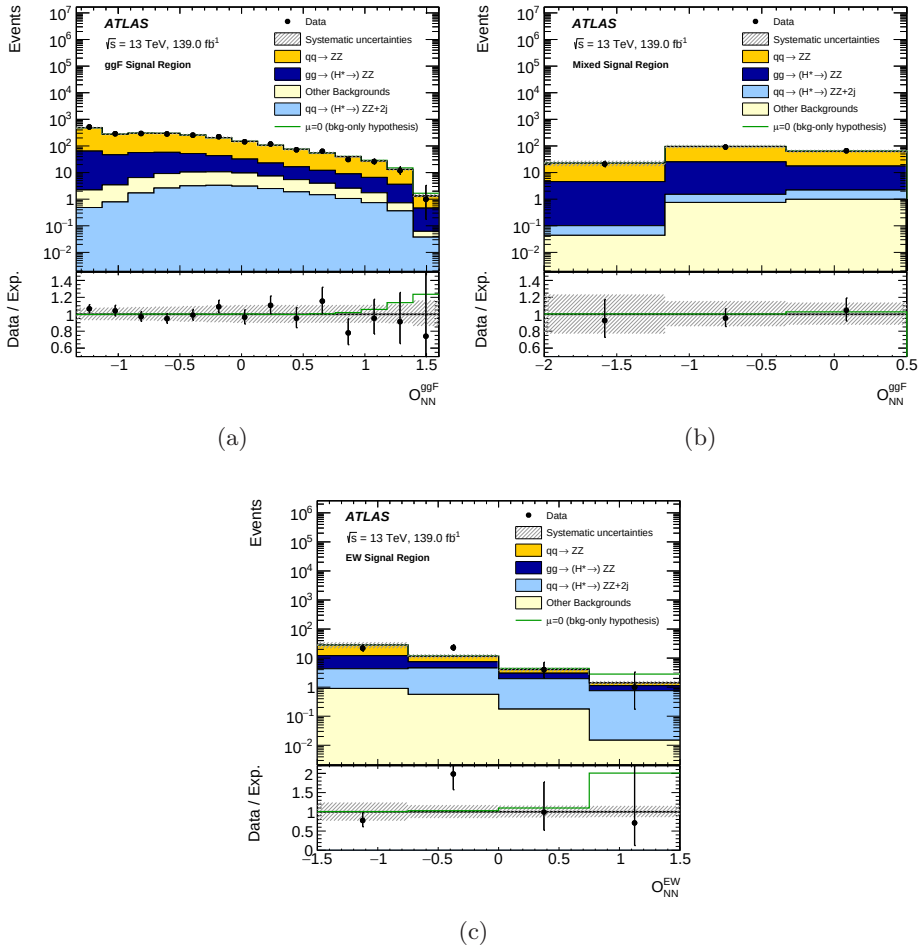

(a) (b)

(c)

Fig. 1.: The expected and observed Standard Model distributions in the 4ℓ channel for (a) $\mathcal{O}_{\mathrm{NN}}^{\mathrm{ggF}}$ in the ggF signal region, (b) $\mathcal{O}_{\mathrm{NN}}^{\mathrm{ggF}}$ in the mixed signal region, and (c) $\mathcal{O}_{\mathrm{NN}}^{\mathrm{EW}}$ in the EW (VBF+VH) signal region. The lower panel of each plot presents the ratio of data to expectation (black points) and the total systematic uncertainties (hatched area), as well as the ratio of no off-shell Higgs or background only to expectation (green curve).

The cross-section distributions against the neural network discriminant are presented in fig. 1.

2˙2. $ZZ \to 2\ell 2\nu$ *Analysis*. – The $2\ell 2\nu$ channel consists of a pair of leptons and significant missing transverse energy $E_{\mathrm{T}}^{\mathrm{miss}}$ (resulting from undetectable neutrinos) in its final state. The $2\ell 2\nu$ channel has a six-times larger branching ratio (prior to event selections) than the 4ℓ channel, but it is exposed to larger and more complex backgrounds.

Similar to the 4ℓ analysis, three SRs are designed to enhance sensitivity in both ggF and EW production modes in $2\ell 2\nu$. The dominant background is $q\bar{q} \to ZZ$ events, which is estimated from the $ZZ \to 4\ell$ analysis. The estimation of the WZ background

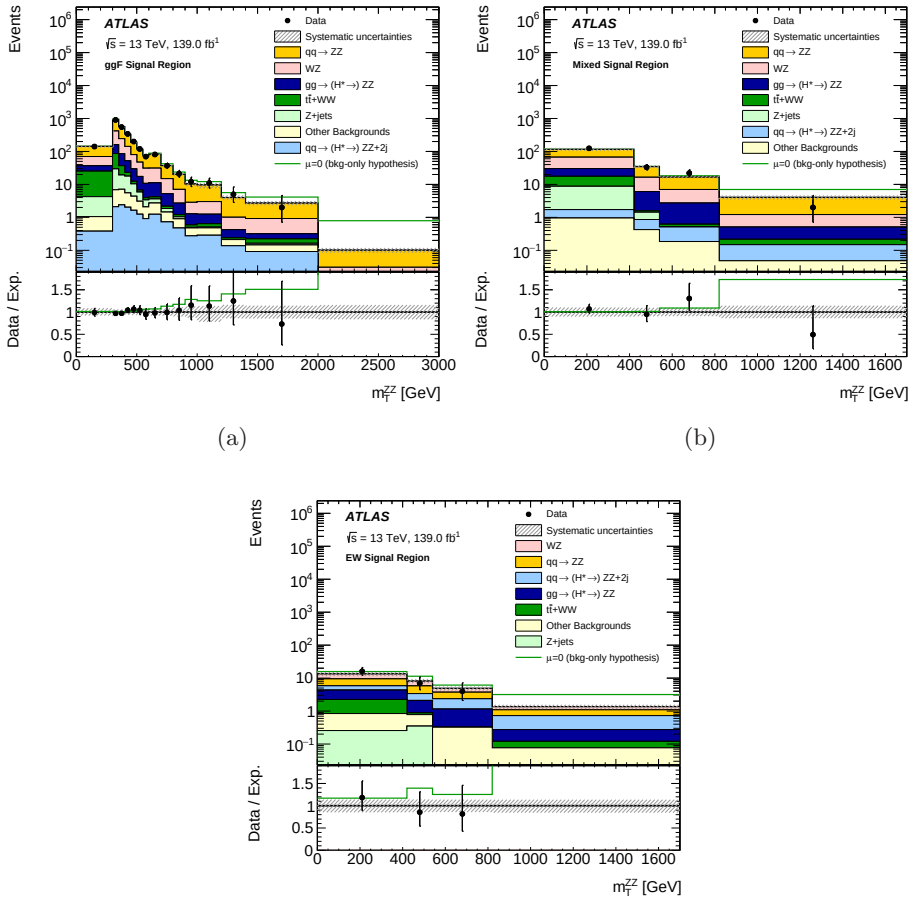

(a) (b)

(c)

Fig. 2.: The expected and observed SM m_{T}^{ZZ} distributions in the $2\ell 2\nu$ channel for (a) the ggF SR, (b) the mixed SR, and (c) the EW SR. The lower panel presents the ratio of data to expectation and the total systematic uncertainty (hatched area), as well as the ratio of no off-shell Higgs or background only to the expectation (green curve).

in the SRs employs a dedicated WZ CR, where the purity of the WZ events is more than 90%. The non-resonant $\ell\ell$ background from single-top, $q\bar{q} \to WW$ processes, or $t\bar{t}$ is estimated from the $e\mu$ CR, where an opposite-sign $e\mu$ is required to differentiate from SRs. Backgrounds from Z+jets, tri-boson, and $t\bar{t}V$ production are estimated from MC simulations.

The transverse mass, m_{T}, is utilized as the discriminant variable:

$$m_{\mathrm{T}}^2 = \left[\sqrt{m_Z^2 + |\vec{p}_{\mathrm{T}}^{\,\ell\ell}|^2} + \sqrt{m_Z^2 + |\vec{E}_{\mathrm{T}}^{miss}|^2}\right]^2 - \left[\vec{p}_{\mathrm{T}}^{\,\ell\ell} + \vec{E}_{\mathrm{T}}^{miss}\right]^2 \quad (4)$$

where m_Z is the Z boson rest mass.

TABLE I.: Ranking of dominant systematic uncertainties in the combined off-shell 4ℓ and $2\ell 2\nu$ channels. The second column shows the value of $\mu_{\text{off-shell}}$ at the upper two standard deviation confidence intervals ($-2\ln\lambda = 4$) when the corresponding systematic uncertainty in the first column is removed from the fit. Generally, the smaller the value of $\mu_{\text{off-shell}}$, the greater the impact of the systematic uncertainty.

Systematic Uncertainty Removed	$\mu_{\text{off-shell}}$ $(-2\ln\lambda = 4)$
Parton shower uncertainty for $gg \to ZZ$ (normalization)	2.26
Jet energy scale and resolution uncertainties	2.26
NLO EW uncertainty for $q\bar{q} \to ZZ$	2.27
Parton shower uncertainty for $gg \to ZZ$ (shape)	2.29
NLO QCD uncertainty for $gg \to ZZ$	2.29
Parton shower uncertainty for $q\bar{q} \to ZZ$ (shape)	2.29
None	2.30

3. – Results

The statistical model used in this analysis is based on the profiled likelihood method [8]. A binned likelihood, as a product of the Poisson distribution of all bins, is fitted simultaneously in the SRs and CRs.

The theoretical and experimental uncertainties in this likelihood follow Gaussian distributions, which are constrained by theoretical calculations and auxiliary measurements. These systematic uncertainties are correlated between the two channels where suitable. The uncertainties from the finite MC simulation are modelled as Poisson distributions. Dominant systematic uncertainties are listed in table I. Generally, the smaller the value of $\mu_{\text{off-shell}}$ at $-2\ln\lambda = 4$, the greater the systematic uncertainty impact.

To constrain the overall signal strength of the off-shell Higgs $\mu_{\text{off-shell}}$, the signal strengths in the two production modes are assumed to be equal $\mu^{\text{ggF}}_{\text{off-shell}} = \mu^{\text{EW}}_{\text{off-shell}} = \mu_{\text{off-shell}}$. The result is presented in fig. 3(a). The best-fit signal strength $\mu_{\text{off-shell}}$ is $1.1^{+0.7}_{-0.6}$ for observation. The observed (expected) no off-shell Higgs boson is rejected at 3.3 σ (2.2 σ), marking evidence of the off-shell Higgs boson.

The off-shell analysis is combined with the on-shell Higgs to 4ℓ analysis [7] to provide Higgs width constraints if the off-shell to on-shell Higgs-gluon and Higgs-Z boson coupling are assumed to be equal. The result is presented in fig. 3(b) and the best-fit Higgs width Γ_H is $4.5^{+3.3}_{-2.5}$ MeV, calculated from the measured $\Gamma_H/\Gamma_H^{\text{SM}}$ with $\Gamma_H^{\text{SM}} = 4.07$ MeV. The observed (expected) lower and upper limits at 95% confidence level for the Higgs width are $0.5\ (0.1) < \Gamma_H < 10.5\ (10.9)$ MeV.

4. – Conclusion

This paper reports a search for off-shell Higgs production measurements in the 4ℓ and $2\ell 2\nu$ channels using the full Run-2 dataset at ATLAS. This analysis accounts for both gluon-gluon fusion and electroweak (vector-boson fusion and VH) production modes. The

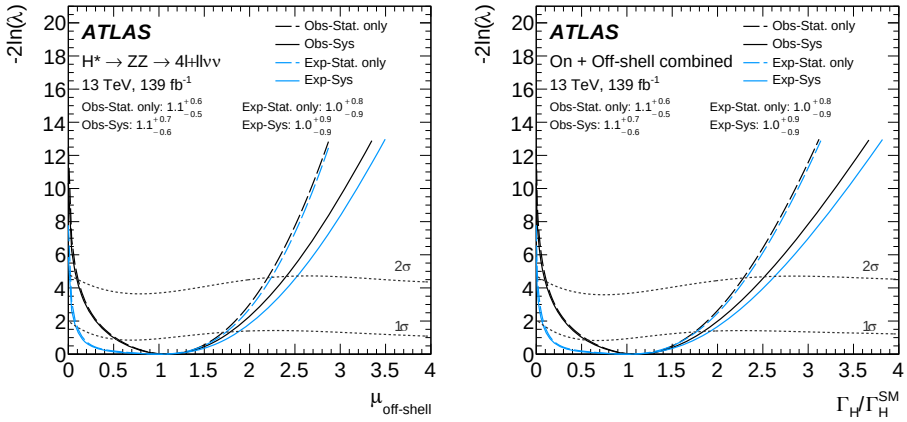

(a) (b)

Fig. 3.: Negative log-likelihood profile, $-2\ln\lambda$, as a function of (a) off-shell Higgs signal strength $\mu_{\text{off-shell}}$, and (b) $\Gamma_H/\Gamma_H^{\text{SM}}$. Dotted curves represent the one- and two-standard deviation confidence intervals obtained from the Neyman construction.

background-only (or absence of the off-shell Higgs boson) is rejected at the confidence level of 3.3 σ (2.2 σ) for the observed (expected) result, marking evidence of off-shell Higgs production. No significant deviation from the SM prediction is observed within the uncertainties. The Higgs boson decay width is measured as $4.5^{+3.3}_{-2.5}$ MeV and the upper limit is 10.5 MeV at the 95% confidence level, obtained from the combination of off-shell and on-shell Higgs boson analyses.

REFERENCES

[1] ATLAS Collaboration, *Phys. Lett. B*, **716** (2012) 1.
[2] CMS Collaboration, *Phys. Lett. B*, **716** (2012) 30.
[3] ATLAS Collaboration, *Nature*, **607** (2022) 52.
[4] CMS Collaboration, *Nature*, **607** (2022) 60.
[5] LHC Higgs Working Group, CERN-2017-002-M, Vol. **2** (2017) 10.
[6] Caola F. and Melnikov K., *Phys. Rev. D*, **88** (2013) 054024.
[7] ATLAS Collaboration, *Eur. Phys. J. C*, **80** (2020) 957.
[8] Cowan G., Cranmer K. *et al.*, *Eur. Phys. J. C*, **77** (2011) 1554.